Contrib. Plasma Phys. **45**, No. 8, 553 – 567 (2005) / **DOI** 10.1002/ctpp.200510061

Heterogeneous Plasma-Producing Structures at Current Implosion of a Wire Array

E. V. Grabovsky, K. N. Mitrofanov, S. L. Nedoseev, G. M. Oleinik, I. Yu. Porofeev, A. A. Samokhin*, and **I. N. Frolov**

SRC RF TRINITI, 142190,Troitsk, Moscow Reg.

Received 23 March 2004, accepted 7 April 2005
Published online 25 November 2005

Key words Exploding wires, heterogeneous structures.
PACS 52.80.Qj, 52.70.La, 64.75.+9

Characteristic properties of the plasma production process have been considered for the case of megampere currents flowing through hollow cylindrical wire arrays of the Angara-5-1 facility. In 3-4 nanoseconds after voltage applying to the wire surfaces there appear a plasma layer. The system becomes heterogeneous, i.e. consisting of a kernel of metal wires and a plasma layer. In several nanoseconds the current flow goes from metal to plasma, which results in reducing the electric field strength along the wire.

The Joule heat energy delivered to the metal before the moment of complete current trapping by plasma is insufficient for the whole mass transition to a hot plasma state. The X-ray radiography techniques made it possible to detect and study dense clusters of substance of $\sim$1g/cm^3 at a developed discharge stage. The radial expansion velocity of $\sim 10^4$ cm/s measured at the 70-th nanosecond after the current start allows treating the dense core at a late stage in the form of a submicron heterogeneous structure from its liquid and slightly ionized gas phase.

1 Introduction

The implosion of cylindrical arrays from micron-size tungsten and aluminum wires (liners) under the action of nanosecond current pulses has been investigated earlier[1, 2] and is still under study [3, 4]. As a result of current compression of a wire array material a Z-pinch develops. At its final stage there appear a high -power pulse of soft X-radiation, that is of importance for CTF [5], the investigations into fundamental properties of matter in extreme conditions [6], etc.

In early works with wire arrays a phenomenon of carrying a low-dense plasma and current towards the center of the system when affected by the Lorentz force has been revealed [1]. The process was considered to be interfering in compact compressing a wire liner by a collective magnetic field because of the transfer of a part of current and mass to the center and the pre-pinch formation. It was supposed, that for a great number of wires any negative consequences could be moderated due to a fast formation of a continuos and nearly homogeneous shell of an imploded wire plasma [7]. It was also considered, that the self-magnetic field of the current flowing through the wire was high enough to compensate a heat pressure and to limit the plasma layer radius around the wire in the array [8].

A better understanding of the spatial-time structure of plasma fluxes and material distribution in the multiwire array has been gained in [9,10]. A concept of a prolonged plasma production process, as an alternative to a 0-dimensional model and shell models for wire arrays, is presented as a dependence of the plasma velocity on the fixed inner surface of the liner upon the full current J and the velocity of the plasma inflow *dm/dt* to the inner volume [11]. The relation expresses the law of conservation of momentum, complimented with a condition for Mach number (M_A=1) for a thin dissipative boundary layer (ohmic).

There still exist an uncertain role of the electron emission at a fast Joule heat up in both arising a primary plasma on the wire surface [12, 13] and subsequent producing of plasma from the products of electric wire

* Corresponding author: e-mail:samokhin@triniti.ru

implosion. As to the latter, natural energy sources to ionize a cold substance are: a thermal energy (transferred by heat conduction) of a plasma flux [11], an energy of pre-pinch radiation [15] and an energy of the electric field in the point of the wire location. The model with heat conduction gives a dependence of *dm/dt* on J, that is true only for an initial discharge phase. A constant of proportionality, which includes the energy value of ionization (price of plasma production), can be determined from the comparison with the experiment.

For the first time, the heterogeneous structure of the explosive wire core was detected using an X-ray diagnostics with an X-pinch technique for both a single wire [16] and an array [17]. The spatial (r, z)-structure of the plasma shell and the core of tungsten and titanium wires in a self-magnetic field is simulated numerically within the system of equations of two-dimensional radiation magneto-hydrodynamics, on passing a shock wave through a designed discontinuity of the density (1:50) on the disturbed cylindrical border of the plasma and the one-phase liquid core [18].

Recently, the electric explosion of a single thin wire at a high rate of current rise has become a subject of an active experimental study [19, 20, 37]. The expansion velocity of the exploding wire ranging from 0.2 μm/ns (titanium) to 5 μm/ns (zinc) is given in [19], dependent on the specific resistance of the material and the energy input at the stage of Joule heating in $\sim$50-60 ns at a current density rise of $\sim$4 MA cm^{-2}/ns. For a significantly faster discharge ($\sim$50 MA cm^{-2}/ns) the expansion velocity of the tungsten wire 0.6 μm/ns [20] is nearly twice as large as that in [19] (0.35 μm/ns).

Nevertheless, on the Angara-5-1 facility in the experiments with multiwire tungsten arrays [21] for first 10 ns the current density derivative is around 500 MA cm^{-2}/ns that is by an order of magnitude greater than in [20]. From the comparison of the data in [19 and 20] (in the logarithmic scale), it follows that, for operation conditions of [21], the expansion velocity should increase two times and achieve $\sim$1.2 μm/ns. A verification of this estimate of the core expansion velocity seems to be especially urgent due to the presence of a strong collective magnetic field, which disturbs a cylindrical symmetry of a single wire. Not only quantitative differences can be expected, but, first of all, qualitative ones, since the interaction between the core and the plasma that drifts towards the center under the Lorents force proves to be much slighter than that in the experiment with a single wire.

At the current compression of nested wire arrays an attainable Z-pinch state is characterized by regularity of its reproducibility and a better, as against a single array, uniformity [22-25]. At present, attention is focused on the study of the inner and outer array interaction [26]. The magnetic field measurements taken outside, inside and between the arrays on the Angara-5-1 facility enable us to elucidate some details of this interaction, while the visualization of wire kernels using an X-ray radiography technique makes it possible to elicit their inner structure.

2 Experimental design

Cylindrical single and double wire arrays 8-20 mm in diameter and 10-15 mm high were used as wire liners in the present work. The diameter of the tungsten wires ranged from 4 to 10 μm. The arrays were placed in a vacuum chamber of the Angara-5-1 facility [17]. The chamber was pumped down to 10^{-5}torr with a diffusion oil-vapor pump. A pre-pulse of the generator was suppressed by a pre-pulse spark gap located just in front of the liner. At the pre-discharge stage the field strength on the array was not in excess of 10V/cm, the temperature increase of the wires was less than 10^{o}C for this time.

The results of two experimental runs are given in the work. In one of the runs a magnitude of the electric field on the wire surface was studied for the first $\sim$5-15 ns period of the current flow through the array. In the second run of the experiments dense cores were studied in 60-80 ns after the current start.

2.1 Initial current flow stage

The liner comprising 8 (or 16) wires was included in the Angara-5-1 facility. With the aim of studying an initial discharge phase current and voltage were simultaneously measured directly in the array. A shunt with a time resolution of 5 ns was used to take current. To measure voltage a resistive divider was coaxially connected to the anode and, by use of a metal rod 0.1 cm in diameter placed strictly along the liner axis, to the cathode (Fig. 1). The time resolution of the divider was 2 ns.

The voltage on the divider differs from that on the wire in question by having an inductive component for the contour formed by this wire and conductors connecting the divider. The peculiarity is that the inductive component is small and may be neglected. The optic frame system based on an MKP camera intended to detect

the wire array image had a 10 ns time gate. The spatial resolution on the object was 40 μm with a depth of focus of about 2 mm. The dynamic detection range of the system was $\sim$20.

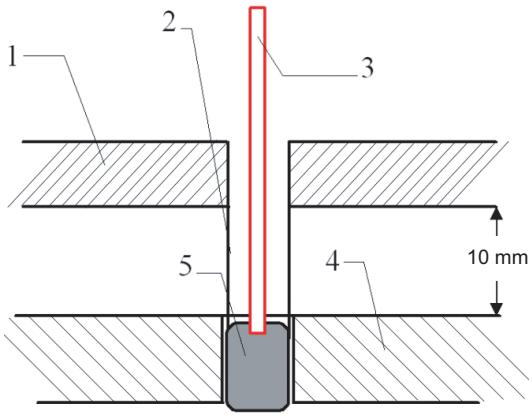

Fig. 1 Circuit diagram of the wire array and the voltage divider. 1 - anode, 2 - wires, 3 - metallic rod to connect voltage divider to cathode, 4 - cathode, 5 - cathode electrode of wire array.

2.2 Wire radiography at the developed stage of implosion

In the second run of the experiments the probing of the nested arrays was performed by making use of the X-pinch radiation on the Angara-5-11 facility at a current discharge of $\sim$3 MA [28]. A double coaxial array from identical tungsten wires 6 μm in diameter was under study. The diameters of the outer array of 40 wires and the inner array of 120 wires were 20 mm and 12 mm, respectively.

The scheme of the experiment on probing multiwire nested arrays is shown in Fig. 2. Passed through the object in question the X-pinch radiation was detected by a photographic film. The adjustment was made in such a way, that an image of the inner and outer areas of the inner array appeared on the film. The film was 1.2 m from the X-pinch.

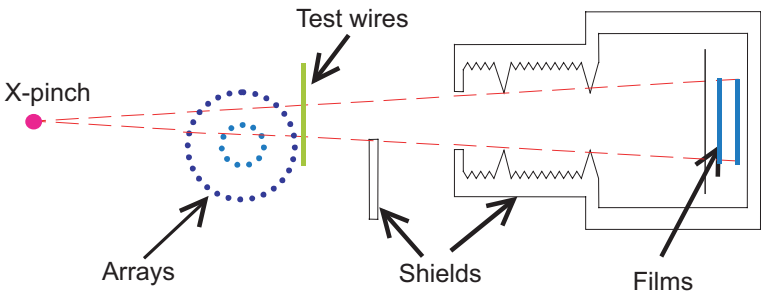

Fig. 2 Layout of techniques for radiographic measurements.

The X-pinch looked like four symmetrically crossed in the middle molybdenum wires 20 μm in diameter. The X-pinch substituted one of the eight reverse current leads at the distance of 45 mm from the axis and was connected in series with the liner [29]. The energy of the X-pinch radiation in the X-range exceeded 200 mJ per pulse. The radiation was detected by films RF-3, UF-SC. A 10 μm aluminum filter was placed in front of the films. An image was formed in quanta with an energy of > 1.5 keV.

For the purpose of transiting from film blackening to the density of the tungsten liner a step attenuator of tungsten filters with their density from 300 to 1300 μg/cm^2 was placed in front of the film. The shadows from the filters were detected on the same films as the ones from the liner in the X-ray quanta. The spatial resolution of the technique was limited by a diffraction divergency and equaled to 4 μm. With the aim of control some test wires 5 μm in diameter with no current were placed near the liner and reliably detected (Fig. 2).

3 Experimental Results

3.1 Break-down along the wire surface

The temporal voltage profiles on the axis are given in Fig. 3 for several shots with tungsten wire arrays and one no-load run (with no array). In the absence of the load for 50 ns the voltage is equal to the output voltage of the generator. Detected for first 20 ns the maximum voltage value varied within 5 to 18 kV for various liners, which differed in their diameter and the number and diameter of wires. The values of maximum voltage proved to be considerably less, and the pulse lengths shorter, than those measured at no load.

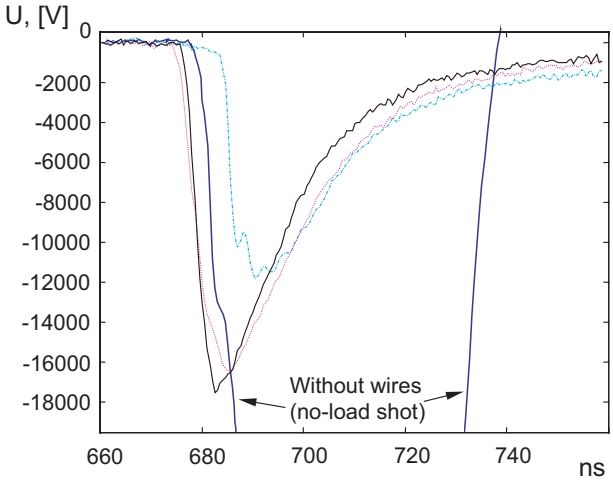

Fig. 3 Voltage on the liner axis $U(t)$ for several shots with the wire array and for one shot of no-load condition.

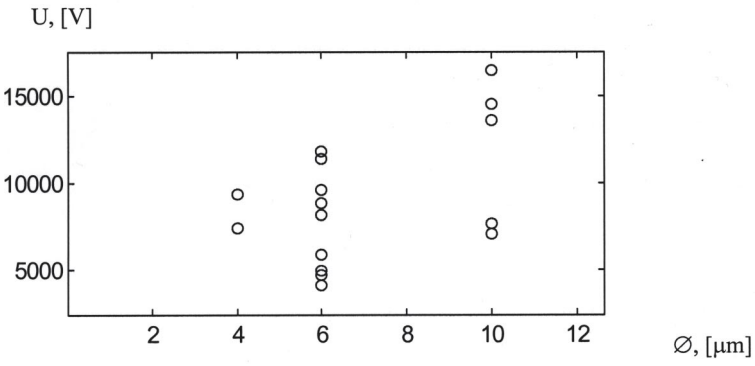

Fig. 4 Maximum amplitude of voltage U on the liner axis against diameter of tungsten wires in the array.

Fig. 4 shows the maximum voltage on the array against the tungsten wire diameter. If outer upper points be taken into account, one can state, that maximum voltage amplitudes increase with the wire diameter.

In all the experiments performed the load resistance for first 10 ns proves to be a on monotonic function of time. Its maximum value calculated in terms of the voltage and current measured was always several times less, than the liner resistance at the tungsten melting temperature. The high conductivity can be easily explained by a shunting effect of a near-surface plasma [12]. A typical temporal dependence of the voltage $U(t)$ on the axis and the current $J(t)$ referred to a single wire is given in Fig. 5 (the liner of eight tungsten wires $\emptyset$10 μm, 1cm high, and 8 mm in diameter). The bottom part of this Figure shows, in term of a single wire, the load resistance U/J, the calculated wire resistance R_w and the near-surface plasma layer (shunt) resistance R_{pl}=$(J/U\text{-}1/R_w)^{-1}$. The temporal wire resistance $R_w(t)$ was calculated for the initial radius and length of the wire in terms of a known temperature dependence of the specific resistance of tungsten and the measured voltage $U(t)$.

The current and voltage on the load make it possible to calculate the energy input to the wire due to Ohmic heating for first 2-3 ns. The tungsten temperature obtained at the time moment determined by divergency between

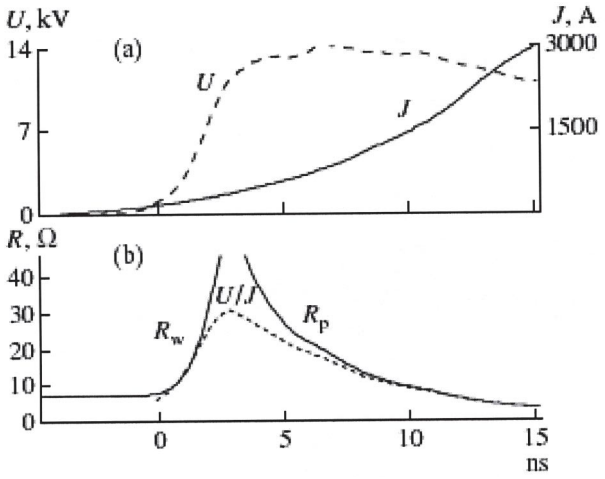

Fig. 5 (a) Waveforms of the voltage $U(t)$ across an 8-mm diameter wire array consisting of eight 10-μm tungsten wires and the current through one wire $J(t)$. (b) Time evolution of the resistances (per one wire) calculated from the voltage and current waveforms: the total load resistance $U(t)/J(t)$, the wire resistance $R_w(t)$, and the resistance of the surface plasma $R_p(t)$.

the load resistance and the calculated one does not exceed 2000^{o}C for the majority of the shots. The given temperature is lower than that of tungsten melting (3380^{o}C).

Taking into account, that the tungsten resistance at a powerful electric heat up of the wire depends upon non-controlled and insufficiently investigated processes, one can positively state the fact of plasma appearance at the moment of the resistance maximum achieved (Fig. 5). The plasma appearance is due to evaporation of surface impurities with a small atomic weight [31], and, likely, with presence of oil traces on the wire surface [9]. A preliminary liner heat up in vacuum up to red glow did not practically affect the wire array impedance at the discharge start.

A break-down of the formed gas layer can be influenced by electron emission amplified by the fact that on a certain part of a thin wire for a certain electrode configuration the radial electric field can be 10-100 times as high as the axial field [32].

3.2 Wire radiography in the process of implosion

Fig.6 presents synchronized signals of current through liner, soft X-radiation of Z-pinch and X-pinch flash. The flash of the probing radiation occurred 80 ns before the maximum Z-pinch radiation. The results of probing the wire array by X- pinch rays are given in Fig.7. In its upper part Fig.7 shows a fragment of a shadowgraph obtained as a result of this probing. Thin sloping light lines in right bottom corner of the Figure is a shadow from the test wire 6 μm in diameter.

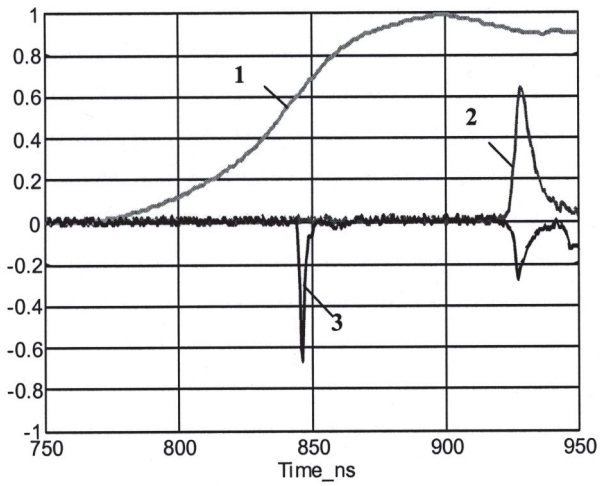

Fig. 6 Oscillograms: 1 - discharge current (1 MA/div), 2 - profile of Z-pinch SXR (a.u.), 3 - profile of X-pinch radiation (a. u.).

The shadowgraphs of the step attenuator from tungsten with a known areal density allow the plasma density in various liner points to be evaluated. Further, there will be used such a characteristic of the mass distribution as the areal density ρl [μg/cm^2], that is equal to the integral of volumetric density along the probing ray.

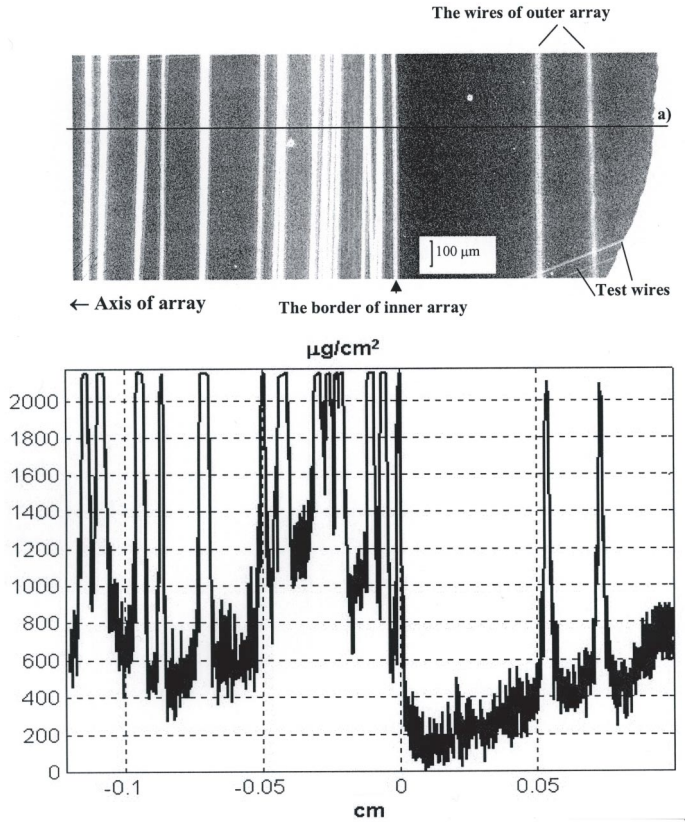

Fig. 7 Radiography data. At the top - shadowgraph of part of the outer and inner arrays At the bottom left: plot of integral along the probing beam plasma density.

In the bottom part of Fig.7 the treatment results of the wire array shadowgraph in the process of implosion are presented. The radial profile of the areal density ρl for a straight line a) was calculated using the detected film blackening density in the upper part of Fig. 7. The abscissa in the bottom part of Fig. 7 is oriented from left to right on the radius from the system center. The 0-coordinate corresponds with the border of the inner array and the coordinate of its axis is -0.6 cm.

The sharp peaks in the distribution of the areal density (Fig. 7) correspond with dense cores. To the right from the inner array border a small part of the outer array plasma is seen. The given detected plasma extends from the wires of the outer array in the direction of the axis at a distance of $\sim$800 μm. The plasma border of the inner array is distant not more than 150 μm from the wires (in average) in the radial direction towards the center.

Fig. 8 gives an amplified image of the cores of the outer and inner arrays. These cores have the same diameters. However, in contrast with the wire cores of the inner array, the core from the outer array has a more "spongy" structure. The core of the outer array are cut in the axial direction with an interval of $\sim$20 μm. The same structure of cores was observed at implosion of single arrays. A detailed profile of the areal plasma density in the vicinity of one of the dense cores of the inner liner is shown in Fig. 9. The major fraction of the substance from the inner array wires ($\sim$80%) is inside the dense core. The other 20% are distributed in the region $\sim$80-90 μm thick. As to the outer array, the core contains about 60% of the initial wire mass.

In spite of a strong axial non-uniformity and diverse degrees of mass exhaustion, the detected (by quanta with energies $\sim$3 keV) cores of the inner and outer liners have the same diameter $\sim$20μm. An increase in the diameter from 6 μm to 20 μm corresponds, at least, a 10-fold fall of the density.

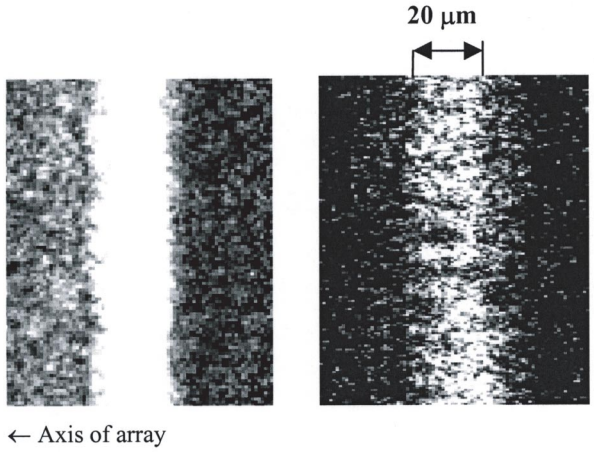

Fig. 8 Shadowgraph of part of wire cores: left - from the inner array, right - from the outer array.

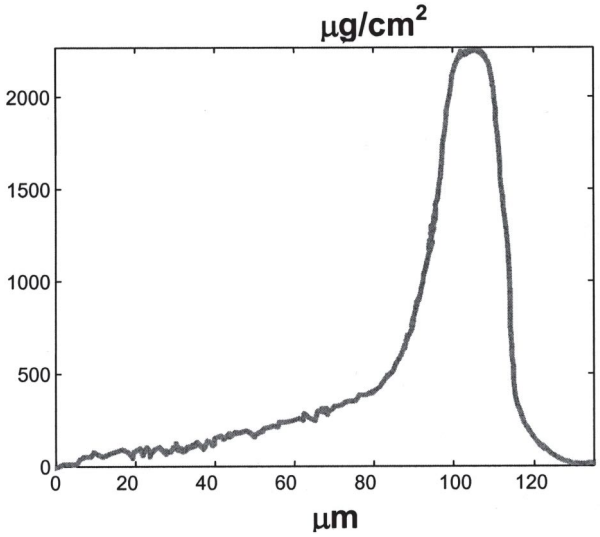

Fig. 9 Profile of areal plasma density near one core of the inner cascade highlighted from image in Figure 7.

3.3 Spatial non-uniformity of breakdown and heterogeneity of cores

To investigate the uniformity of the initial discharge stage (breakdown) frame photography of a single tungsten liner was taken in the X-ray (Fig. 10a, [43]) and in the visible spectrum (Fig. 10b).

The earlier wire glow detected in the X-ray range at the ∼2-nd nanosecond is non-uniform both in the azimuthal and axial direction (Fig. 10a). Only about 5 wires of 48 with a 5 μm diameter can be seen in the array. At this moment the current value for a single wire in the array is 100 A, and for one glowing wire it equals 1 kA. The characteristic size of the plasma formation around the wire in the azimuthal direction is ∼300 μm, that is less, than the space between the wires in the array which is equal to 800 μm.

The image of the eight wire array with the wire diameter of 7,5 μm detected at the moment when the current attained ∼3 kA/wire is presented in Fig. 10b. A characteristic property is a particularly pronounced large-scale axial non-uniformity of emittance distribution along the wires. The images of separate wires are also greatly different. A non-uniform energy input to a wire at an initial cold stage predetermines, later, a not uniform exhaustion of various parts of the core. Such a core with a ∼1 mm size of its non-uniformity is given in Fig. 11.

The core exhaustion non-uniformity develops not only along the axis, but also for different wires in the array. So, Fig. 12 demonstrates an obtained in [33] profile of the areal plasma density ρl near an outer radius of a single array. The X-axis in Fig. 12 is radially directed from right to left to the array center, X=0 at the array surface. In the middle on the plot of the areal density ρl (Fig. 12) one can see two narrow peaks (at X=220 μm and X=550 μm) around 25 μm wide, which correspond with the shadows from two dense cores. To the right from the dense cores two feebly marked humps, which are corresponds two other cores with substance in a low-density

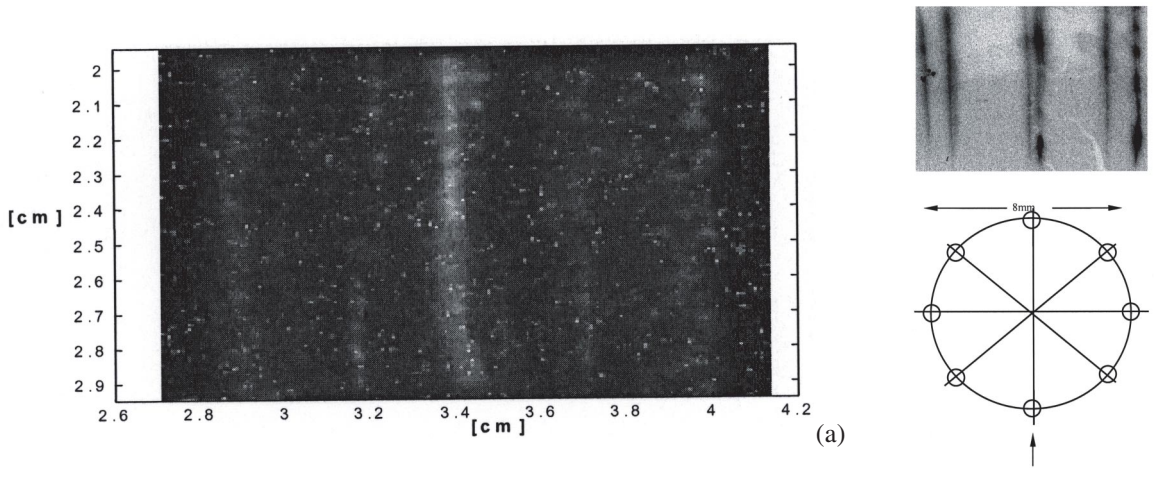

Fig. 10 (a) X-ray image at 2 ns. Liner with diameter 12 mm and height 15 mm. Forty eight wires Ø 5 μm. Resolution is 200 μm for $hv \sim$200 eV. (b) Image detected by optic frame chamber. Current is 24 kA. Liner with diameter 8 mm and height 10 mm. Eight wires Ø 7.5 μm.

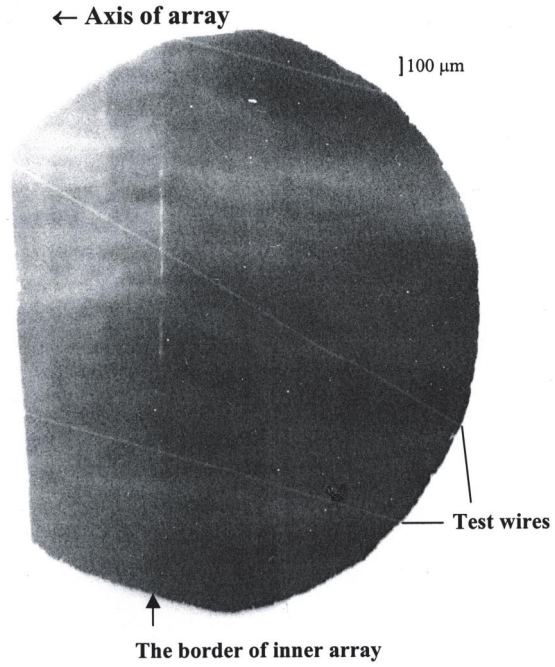

Fig. 11 Shadowgraph in X-ray of the part from inner array. At time 40 ns before maximum of X-radiation. Energy of X-pinch quanta is 1-1.5 keV.

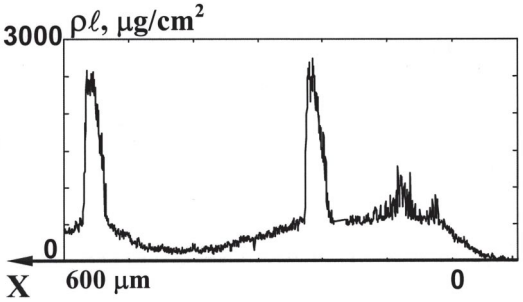

Fig. 12 Density of plasma near the surface of a single array. X-axis is oriented along radius from right to left towards the liner axis. X=0 on the wire array radius.

plasma state.The wire exhaustion at one moment of time is different, that also evidences the difference in the rate of plasma production and is likely due to a non-uniform current distribution over wires in the liner at the initial stage.

4 Plasma surrounding of wire in the liner at an initial discharge stage

The temporal dependencies of the current and voltage on the liner make possible the estimation of produced plasma parameters. Let us consider a cylindrical plasma column around a wire with a Spitzer conductivity

dependent on a temperature T_e and an average ion charge $Z{\sim}T_e^{0.5}$. Assume also that the plasma expands into vacuum with a velocity of ion sound. This model well agrees with the detected voltage and current through the array for $\sim$10 ns for the tungsten plasma with a temperature falling in time from 30 to 20 eV. Fig. 13 shows two resistance values divided by an initial resistance of the liner depending on time. One of them, the experimental one, is calculated on the basis of the detected voltage and current (shown by circles), the second is obtained from the given model for the tungsten plasma with $T_e{\sim}$24 eV.The plasma channel resistance is equal to the initial resistance of the wire at the time moment of $\sim$5.5 ns. In the model presented the velocity of plasma expansion is $0.9{\cdot}10^6$ cm/s. Accordingly, in 10 ns after plasma appearance on the surface the plasma column radius achieves $\sim$100 μm. Note, the given values are independent on the plasma mass of the current channel and not related with the equation of energy, that corresponds with the model of point explosion.

The counterpressure should be taken into account, which is of importance when the plasma radius exceeds the skin-layer thickness. However, since the model considered agrees with the experiment up to 1 kA per wire one can obtain a lower border for the plasma mass and density by equating the expansion velocity of the visible glow border ($0.9{\cdot}10^6$cm/s) to the Alfven velocity. Then in 10 ns after breakdown the plasma mass per one wire exceeds $\sim 10^{-8}$g/cm and the concentration is more than $\sim 10^{17}$ cm^{-3}.

The collective magnetic field in the array is much lower than that of a separate wire on its surface: their ratio is $Nr_w/R \ll 1$, where N is the number of wires, r_w is the wire radius and R is the liner radius. As the pressure of the plasma exceeds that of the self magnetic field, the collective magnetic field does not affect the plasma column expansion, at least, for first ten nanoseconds. In accordance with the probe measurements [19] the current appears on the liner axis (prepinch) in 30-40 ns after the discharge start. The velocity of the plasma flow towards the center, $\sim 10^7$ cm/s, attributed to the collective magnetic field is by an order of magnitude greater than that of the plasma column expansion of a single wire [32].

What is the cause of a large-scale non-uniform plasma distribution over wires detected in the optical range and a violated azimuthal symmetry between them (Fig. 10) is not clear. Nevertheless, the model given makes it possible, on the basis of the measured current-voltage characteristics, to evaluate the temperature, the lower mass border and the tungsten ion concentration in the near-wire plasma (r$\sim$0.01 cm).

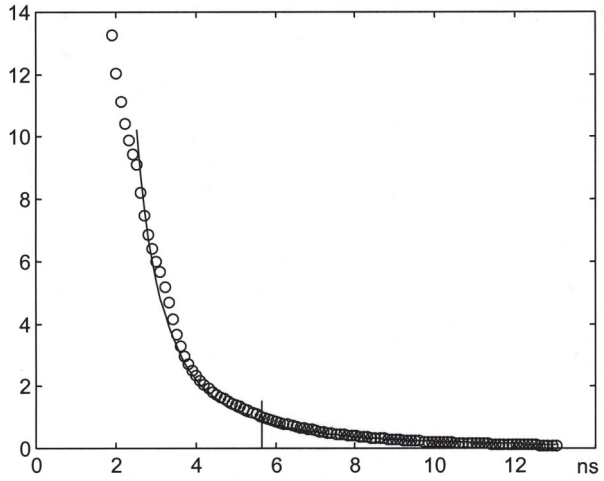

Fig. 13 Resistance of cylindrical plasma layer near wire related to resistance of wire at 300 K. Circles is experiment, solid line- plasma model with T_e varying in time from 30 to 20 eV.

5 Dense cores at a developed discharge stage

The data on the core expansion velocity, 10^4 cm/s, obtained by X-ray probing the wire array with an X-pinch technique [21,23], permits drawing conclusions about the structure of a dense part of tungsten at a rather late time moment (40-70 ns) after the current start. The value of the average density ρ_K of the core substance is 1 g/cm^3, that is less than the critical tungsten density ρ_{CP} =4.5 g/cm^3 [34]. The small expansion velocity $\sim 10^4$ cm/s prevents considering the core as a homogeneous state of a vapour, as the corresponding point in the phase diagram has a temperature of $>$ 12000K and a thermal velocity of $> 8{\cdot}10^4$ cm/s [34]. Under these conditions it is natural to consider the core to be a heterogeneous medium, i.e. a mixture of liquid (drops) and vapour. Note

the velocity of core expansion, observed in the wire array ~0.1 μm/ns, less than in the experiments with a single wire more than one [19,20].

Let us consider a model taking account of evaporation from the surface of the liquid phase and the mass loss by vapour outflow from the core border. The ohmic heating by current J, which flows through an ionized vapour in the core at a specified electric field on the liner "surface", will be taken as an energy source. The electric field strength is evaluated in terms of the model of prolonged plasma production with a thin dissipative boundary layer [11], which separates the dense cores and the hot accelerated plasma of ideal conductivity. Assume, that within this layer the electric field strength is constant and equals $E = 2 \cdot 10^{-9} V J_L / \sqrt{3}\, R_L \sim 50$ (kV/cm). Here, $J_L \sim 2$ (MA) is the full current, $R_L \sim 0.5$ (cm) the liner radius and V$\sim 10^7$ (cm/s) the plasma velocity.

Now we consider a cylindrical cloud of liquid drops, characterized by average radius r_L and a density ρ_L with a number of drops N_L per unit length of core. The linear density of a liquid phase should not be in excess of the corresponding core density. A limitation on the drop concentration $n_L = N_L/\pi\, r_K^2$ follows from the opacity of a heterogeneous structure for X-ray probing: the path length limited by absorption in drop is less than the core radius - $N_L\, r_L^2 > r_K$. So, assuming $\rho_L > 10(g/cm^3)$, we obtain a relation between sizes and densities of the drops and the core:

$$r_L\, \rho_L < r_K \rho_K \quad = \quad 9\,(\mu\text{g/cm}^3) \quad \Rightarrow \quad r_L < 0.9\,(\mu\text{m}), N_L > 1.1 \cdot 10^5 \ \text{(1/cm)}.$$

In terms of the initial wire with its initial radius r_w = 2.5 μm the volumetric concentration of liquid drops, $0.55 \cdot 10^{12}$ (cm^{-3}), is comparable with that of defects in metal, i.e. 10^{12} (cm^{-3}) [36].

The balance equations of mass - m_L, gas - m_G and energy - $m_L\varepsilon_L + m_G\varepsilon_G$ of the liquid in the cylindrical core, on the assumption of the equality of liquid and vapor temperatures, are as follows:

$$m_L/\rho_L + m_G/\rho_G = \pi\, r_K^2, \quad r_L = \sqrt[3]{0.75 m_L/(\pi\, N_L\, \rho_L)}, \tag{1}$$

$$u_T = \sqrt{k_B T/2\pi\, M}, \quad \dot{V} = 2\pi\, r_K\, u_T, \tag{2}$$

$$dm_L/dt = -4\pi r_L^2\, N_L\, u_T(\rho_V(T) - \rho_G), \quad d(m_L + m_G)/dt = \quad -\rho_G \dot{V}, \tag{3}$$

$$m_L\ (d\varepsilon_L\,/\,dt) + m_G\ (d\varepsilon_G\,/\,dt) - (dm_L\,/\,dt)\ (\varepsilon_G - \varepsilon_L) + P_G\,\dot{V} = J\,E. \tag{4}$$

Here, $\rho_V(T)$ is the density of the saturated vapour in the core. The given system is completed with the equation of state [34,35]. The equilibrium degree of gas ionization was calculated with due account of corrections for plasma non-ideality [37], and the core conductivity within the model of an effective Coulomb logarithm [38]. The influence of the liquid disperse phase on the current flow in the tungsten plasma [39] was neglected, that imposes, in particular, restriction on the liquid and gas volume - $m_L/\rho_L < m_G/\rho_G$.

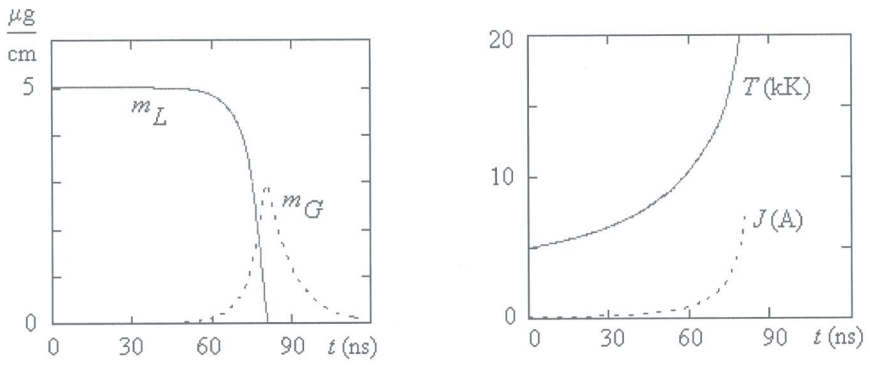

Fig. 14 Mass of liquid and gas phase (left), temperature and current of core (right). N_L=3·10^5 cm^{-1}, r_K=10 μm, E=30 kV/cm.

Fig.14 presents the results of simulation the dynamics of a heterogeneous core in the frames of the equation system (1-4) at constant values of radius r_K=10 μm and field strength E = 30 kV/cm and at initial conditions

T=5000 K, m_G=0 and m_L= 5 μg/cm. The results are given in Fig.15 in view of the dependence on time of the core radius, increasing at a constant velocity, and the field strength growing when initial conditions are T=5000K, m_G=3 μg/cm and m_L= 2 μg/cm. The specific conductivity of plasma when being heated fell down from 100 to 10 $\mu\Omega$.cm. The interpretation of the experimentally observed dense formations of tungsten in the form of a non-equilibrium mixture of liquid drops and gas (plasma) described by the system (1-4) corresponds with the duration of the plasma production process in the wire array, in spite of significant simplifications of the complicated picture of phenomena occurred in the near-critical point [39,40]. The total evaporation of the liquid phase on the periphery of liner, due to Ohmic heating by 80 ns (Fig. 14, 15), corresponds with the transition to qualitatively new state of the plasma implosion process to the discharge axis.

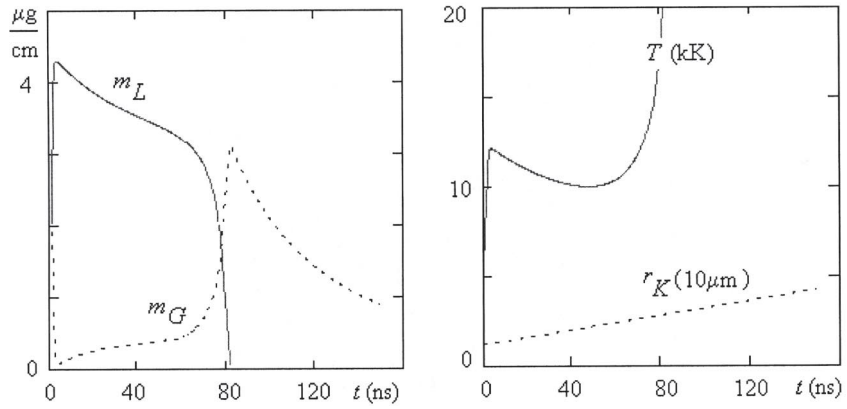

Fig. 15 Mass of liquid and gas (left), core temperature and radius (right). N_L=3·10^5 cm^{-1}, dr_K/dt=0.25 (μm/ns), field strength E is increasing from 10 to 50 (kV/cm) by 80-th ns.

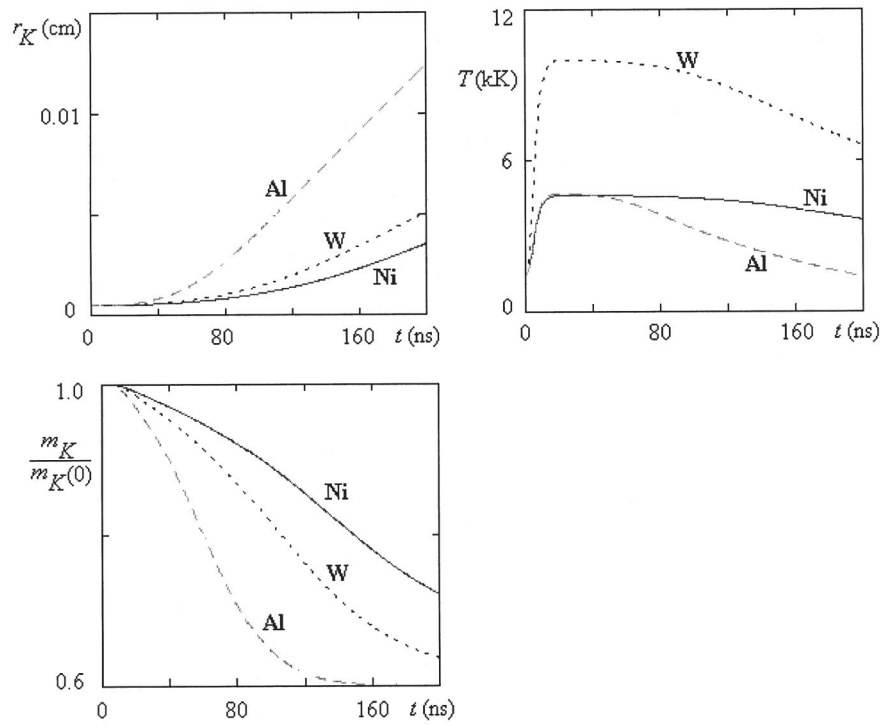

Fig. 16 Mass of liquid and gas (left), core temperature and radius (right). N_L=3·10^5 cm^{-1}, dr_K/dt=0.25 (μm/ns), field strength E is increasing from 10 to 50 (kV/cm) by 80-th ns.

Within the system (1-4) completed with the equation for the core expansion velocity due to an inner thermal pressure (0D- approximation) one can find the core radius $r_K(t)$ for a specific value of energy input Q in the process of wire explosion. Specify the power as a function of $W(t)$=0.5$Qt_o^{-1}\,(t/t_o)^2\,\exp(-t/t_o)$, t_o=2 ns, then the duration of the energy input is $\sim 5t_o$=10 ns. For the experimental data obtained on MAGPIE (1 MA current, 240 ns duration [14]) we determine Q by adjusting for the core expansion velocity in the wire array from tungsten, nickel and aluminum. The core radius, temperature and mass dependence upon time for the three metals is shown in Fig. 16. The energy of electric explosion of wire referred to that of evaporation, Q/Q_B, of tungsten, nickel and aluminum equals 0.45, 13 and 0.42, respectively. Note good agreement of the calculated values of Q/Q_B for nickel and aluminum with the data from another experimental work [17], performed for single thicker wires. This fact may be treated as evidence of a qualitative consistency of the formed model (1-4) with the phenomenon of the electric explosion of wires at a high current density.

6 A dependence on the wire radius

The measurements of the electric parameters of a discharge through the cylindrical tungsten arrays showed, that in 3-4 ns after the current beginning plasma appears on the wire surface. Possible mechanisms of such fast plasma formation are contributed to an anomalous electron emission at current densities j > 1 MA/cm^2 [12], gas desorption from the surface at a temperature of $\sim$700 K and a radial electric field [31]. The effect of the electrode polarity on the electric explosion of wires was demonstrated in [32], the comparison the characteristics of breakdown occurred in gas and along a thin tungsten wire are presented in [42].

In the case of a continuous liner, the geometry of the chamber in the Angara-5-1 facility corresponds with a slightly pronounced negative polarity ($E_r/E \sim 0.001 - 0.01$). As to a wire array a radial component of the electric field on the surface of a thin wire E_r many times increases and is comparable with the longitudinal field strength E. Now we analyze the influence of a moderate radial field directed to the wire upon the absorption of the emitted electron energy on the surface depending on radius.

The motion of an electron emitted from the wire surface at an initial energy ε_s [eV], depends on the wire radius, a longitudinal and radial component of the electric field and a magnetic field on the surface. Let us introduce dimensionless strengths of the electric field - g, g_r and a dimensionless initial electron velocity - g_s

$$g = (eE/m_e)/(r_w\varpi_c^2) = 45.2\ (\Omega/Jr_w),\ g_r = kg,$$
$$g_s = \sqrt{2\varepsilon_s/m_e}/(r_w\varpi_c) = (16.7\ \sqrt{\varepsilon_s}/J).$$

Here, ϖ_c is the cyclotron electron frequency on the wire surface, Ω [Ohm·cm] is the specific resistance, J[A] is the wire current, and k = -E_r/E >0 is the geometrical factor dependent both on the chamber itself [32] and the liner, and the axial wire uniformity. Without regard to the influence of a longitudinal field, $g \ll g_r$, and also a longitudinal component of the initial velocity, the maximum distance covered by the emitted electron over the radius r_* (point of reflection) and the magnitude of its drift along the wire - z_*, in the point of returning to the surface, are equal to

$r_* = r_w\ exp\ (g_r + \sqrt{g_r^2 + g_s^2})$, z_* = $\pi\ (r_* - r_w)\ \Phi(g_r, g_s)$.

At case g_s = 0 the function Φ can presented as $\Phi(g_r)$ = 1+0.51g_r+0.036g_r^2, with accuracy $\sim$0.5% for interval (1< r_*/r_w <30). For a thick titanium wire 20 μm in diameter, that is considered in [32], at r_*/r_w $\sim$7 the value of z_* is 280 μm. In this case for a field strength of $\sim$20 kV/cm the electron energy on the surface will achieve 560 eV.

Now we consider the case when the geometrical factor $k \sim 1$ and a longitudinal component of the field strength g should be taken into account. At a known current $J(t)$ in wire we find g against time. From the equation of energy, assuming that the specific resistance is a linear function of the energy input - $\Omega = \Omega_o + \Omega'(\varepsilon_w - \varepsilon_{wo})$, we obtain

$$g(t) = 45.2\frac{\Omega_o}{r_w J(t)}\exp\left(\frac{\Omega'}{\pi^2\, r_w^4}\int_0^t J(t')^2 dt'\right) \qquad (5)$$

At comparison of wires with the same density of current j, the parameter $g \sim r_w^{-3}$; if the total current J is the same, then for a wire of a smaller radius the value g will be initially greater because is proportional to r_w^{-1}, and be rising in time much faster due to the exponential index which is proportional to r_w^{-4}.

By solving the equation of motion of an emitted electron in crossed electric and magnetic fields, find a dependence of r_* and z_* on two dimensionless parameters - g, k. The electron energy $\Delta\varepsilon = eEr_w z_*$ can be calculated for a particular wire at a given voltage (or current) pulse. The temporal current and temperature dependence of the tungsten wire of r_w = 2.5 μm for a specified voltage impulse is presented in Fig.17a and the corresponding values of energy $\Delta\varepsilon$ for several values of the geometrical factor k in Fig.17b. In the calculated range the maximum deviation over the radius $r_* < 3r_w$, the displacement along the surface $z_* < 15r_w$. It follows from the calculations that there exits an interval of a $\sim$2 ns duration, after which in subsequent 4 ns for k = 0.5 energy increase of electron $\Delta\varepsilon$ = 17 eV, in subsequent 2 ns for k = 1.0 energy $\Delta\varepsilon$ = 23 eV and for k = 1.5 energy $\Delta\varepsilon$ = 55 eV (extrapolation). A strong dependence of the electron energy on the geometrical factor E_r/E exists in the region of a not too great distortion of field (k = 1, 1.5) with achieving an energy level of $\sim$100 eV for $\sim$5 ns after attaining the maximum current through the wire. Note, for thick wires the parameter g proves to be quite small and a noticeable effect of a radial field on the electron motion is possible just at a large value of the geometrical factor $k \sim$100 [32].

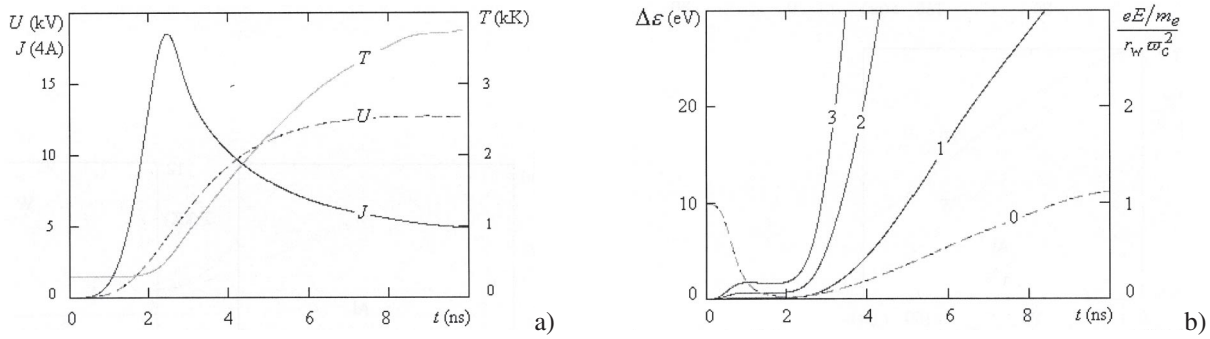

Fig. 17 (a) Voltage, current and temperature of wires for given voltage pulse. Wire radius r_w=2.5 μm. (b) Dimensionless field strength g (0) and energy of emitted electron for values E_r/E = 0.5 (1), 1.0 (2), 1.5 (3).

Let us estimate the electron emission significance for evaporation of tungsten from the surface. The specific power due to absorption of the emitted electrons is $j_s\Delta\varepsilon/\lambda_e\rho$, where j_s is the current density of emission, λ_e is the absorption thickness and ρ is the metal density. For tungsten the current density of thermal emission j_s varies very fast from 14 A/cm^2 at a temperature of 3000 K to 480 A/cm^2 at the temperature of melting [12]. The difference in energy counted from the initial temperature 300 K between these two states is much less than that at the temperature of melting, $\sim$1/5. In our experiments the energy evaluations in terms of Joule heating power are unable to accurately define the wire state at the moment of breakdown over the surface. In the experiments with a slower energy delivery the absorbed energy, up to the moment of shunting the tungsten wire is sufficient for the temperature of melting to be reached [17, 18]. At the density of current emission 480 A/cm^2, the absorption length in metal $\lambda_e = 10^{-3}\mu$m [44] and the electron energy $\Delta\varepsilon$ =100 eV we obtain a specific power of 24 GW/g. An increase of j_s by 100 times, up to an anomalous current density in point of melting [12] is sufficient for evaporation of the surface layer of λ_e thickness in $\sim$2 ns. Note, that the higher the energy $\Delta\varepsilon$, the more acute is the angle (with respect to the surface) of entering the electron into the wire, that results in reducing the thickness of the absorption region and increasing the specific power.

The abnormal emission can be treated as an evidence of anomalous properties of the metal surface at fast heating. [12, 31]. At reducing the wire radius r_w an influence of the surface, including the contribution to the wire resistance; will increase in proportion to $\delta_s/\ r_w$, where δ_s is a certain characteristic thickness on the near-surface layer dependent, in particular, on the manufacturing technique. It can be assumed that the explosion of thin wires $r_w \sim \delta_s$ differs qualitatively from that of thick wires $r_w \gg \delta_s$ both for a single wire and multiwire arrays.

7 Conclusion

In the wire arrays used in superpower generators of X-radiation a heterogeneous submicron structure (a core) containing 70-80% of an initial wire mass is the product of the electric explosion of a thin wire. In spite of strong electric and magnetic fields, a high radiation power and high temperature, the core keeps its substantial properties in the course of the entire process of plasma current compression on the axis governing the rate of substance delivery to the inner array. Such a core is an important element of the whole construction of a self- compressed radiative discharge, both in single and double wire arrays, from the moment of the electric explosion up to the final Z-pinch state.

Unlike the single wires with their plasma not only governing the energy fluxes to the core, but also, by virtue of its inherent instabilities, tends to specify a complicated motion of the central region, the core in the wire array proves to be separated from a direct affect of plasma being carried by a collective magnetic field. For the core on the liner significant are characteristics of the phase diagram and transport properties of metal in the near-critical point, non-equilibrium processes of mass, discharge and energy transfer between liquid and gas components in presence of electric and magnetic fields.

This article is devoted to 60th birthday of V.E. Fortov, and to his outstanding contributions to the physics of strongly coupled plasmas.

References

[1] M.B. Bekhtev, V.D. Vikharev, S.V. Zakharov, et al., Zh. Éksp. Teor. Fiz., **95**, 1653 (1989); [Sov. Phys. JETP, **68**, 955 (1989)].
[2] I.K. Aivazov, M.B. Bekhtev, V.V. Bulan, et al., Fiz. Plazmy, **16**, 645 (1990); [Sov. J. Plasma Phys. **16**, 373 (1990)].
[3] R.B. Spielman, C. Deeney, G.A. Chandler, et al., Phys. Plasmas, **5**, 2105 (1998).
[4] S.V. Lebedev, F.N. Beg, S.N. Bland, et al., Phys. Plasmas, **8**, 3734 (2001).
[5] T.W.L. Sanford, R.E. Olson, R.G. Mock, et al., Phys. of Plasmas, **7**, 4669 (2000).
[6] E.V. Grabovsky, V.P. Smirnov, V.E. Fortov, et al., JETP Lett., **60**, 1 (1994).
[7] T.W.L. Sanford, et al., Phys. Plasmas, **4**, 2188 (1997).
[8] M.G. Heines, IEEE Trans. on Plasma Science, **26**, 1275 (1988).
[9] A.V. Branitsky, E.V. Grabovsky, I.N. Frolov, et al., Proc. 12th Int. Conf. on High-Power Particle Beams (Beams'98), Haifa, Israel. P.599 (1998).
[10] S.V. Lebedev, R. Aliaga-Rossel, S.N. Bland, et al., $40^{\rm th}$ Annual Meeting DPP-APS, New Orleans. 1998.
[11] A.A. Aleksandrov, A.V. Branitsky, G. S. Volkov, et al., Fiz. Plazmy, **27**, 99 (2001); [Plasma Phys. Rep., **27**, 89 (2001)].
[12] S.V. Lebedev, A.I. Savatimsky, Usp. Fiz. Nauk, **144**, 215 (1984); [Sov. Phys. Usp. **27**, 749 (1984)].
[13] A.V. Batrakov, B. Yuttner, S.A. Popov, et al., Pis'ma Zh. Éksp. Teor. Fiz., **75**, 84 (2002).
[14] A.V. Kozirev, A.N. Shishkov, Pis'ma Zh. Tekh. Fiz., **28**, 33 (2002).
[15] S.V. Lebedev, F.N. Beg, S.N. Bland, et al., Phys. Plasmas, **8**, 3734 (2001).
[16] S.A. Pikuz, T.A. Shelkovenko, D.B. Sinars, et al., Phys. Rev. Lett., **23**, 4313 (1999).
[17] I.N. Frolov, E.V. Grabobsky, K.N. Mitrofanov, et al., Proc. of Euro. Conf. (Villa Monastero, Varenna, Italy. Sept. 3-7, 2001) Academic/Plenum Publisher, 257 (2001).
[18] S.Yu. Guskov, G.V. Ivanenkov, A.R. Mingalaev, et al., Fiz. Plaz., **26**, 797 (2000).
[19] K.M. Chandler, D.A. Hammer, D.B. Sinars, et al., IEE Trans. on Plasma Science, **30**, 577 (2002).
[20] G.S. Sarkisov, B.S. Bauer, D.S. De Groot. Pis'ma Zh. Éksp. Teor. Fiz., **73**, 74 (2001); [JETP Lett., **73**, 69 (2001)].
[21] V.V. Alexandrov, I.N. Frolov, M.F. Fedulov, et al., IEEE Transactions on Plasma Science, **30**, 559 (2002).
[22] J. Davis, et al., Appl. Phys. Lett. **70**, 170 (1997).
[23] C. Deeney, et al., Phys. Rev. Lett. **81**, 4883 (1998).
[24] R.E. Terry, et al., Phys. Rev. Lett. **83**, 4305 (1999).
[25] S.V. Lebedev, et al., Phys. Rev. Lett. **84**, 1708 (2000).
[26] S.N. Bland, et al., Phys. of Plasmas, **10**, 1100 (2003).
[27] Z.A. Al'bikov, E.P. Velikhov, A.I. Veretennikov, et al., At. Énerg., **68**, 26 (1990).
[28] V.V. Alexandrov, M.V. Fedulov, I.N. Frolov, et al., Proc. 5th Intern. Conf. Dense Z-pinches. Albuquerque, New Mexico, p91 (2002).
[29] G.S. Volkov, E.V. Grabobsky, I.Yu. Porofeev, et al., Prepr. TRINITI, No 0104A, (2003).
[30] G.S. Volkov, E.V. Grabobsky, M.V. Zurin, et al., Pribory Tekh. Éksp., 110 (2004).

[31] S.M. Karakhanov, Zh. Tekh. Fiz., **48**, 1474 (1978).
[32] G.S. Sarkisov, P.V. Sasorov, K.W. Struve, et al., Phys. Rev. E, **66**, 046413, (2002).
[33] E.V. Grabobsky, K.N. Mitrofanov, I.Yu. Porofeev, et al., Fiz. Plaz., **30**, 139 (2004).
[34] P.R. Levashov, Preprint N1-446 OIVT RAN (2000).
[35] S.I. Tkachenko, K.V. Khishchenko, V.S. Vorobiev, et al., TVT, **39**, 728 (2001).
[36] Issledovanie metallov v zhidkom i tverdom sostoianii. Ed. by I. P. Bardin (Moscow, "Nauka", 1964).
[37] V.E. Fortov, I.T. Yakubov, Fizika neidealnoi plazmy. Acad. Nauk SSSR IVT, (1984).
[38] I.T. Yakubov. Électroprovodnosti neidealnoi plazmy. Usp. Fiz. Nauk **163**, 35 (1993).
[39] A.D. Rakhel, A. Kloss, H. Hess. Int. J. of Thermophysics, **23**, 1369 (2002).
[40] V.N. Korobenko, A.D. Rakhel, A.I. Savatimsky, V.E. Fortov, Fiz. Plaz., **28**, 1093 (2002).
[41] F.N. Beg, S.V. Lebedev, S.N. Bland, et al., IEEE Trans. on Plasma Science, **30**, 552 (2002).
[42] A.G. Russkikx, R.V. Baksht, A.Yu. Labezky, et al., Fiz. Plaz. **30**, 1015 (2004).
[43] V.V. Alexandrov, E.V. Grabovsky, M.V. Zurin, et al., 15^{th} Intern. Conf. On High-Power-Particle Beams, S-Petersburg. July 18-23, p226 (2004).
[44] Fizicheskie Velichiny. Spravochnik. Ed. by I.S. Grigor'ev, E.Z. Meilikhov (Moscow, Énergoatomizdat, 1991).